JOURNAL OF THE ROYAL SOCIETY Interface

J. R. Soc. Interface (2011) **8**, 1815–1824
doi:10.1098/rsif.2011.0240
Published online 1 June 2011

Patterning as a signature of human epidermal stem cell regulation

Allon M. Klein[1,2,*], Varvara Nikolaidou-Neokosmidou[3], David P. Doupé[3], Philip H. Jones[3] and Benjamin D. Simons[1,4,*]

[1]*Cavendish Laboratory, JJ Thomson Avenue, Cambridge CB3 0HE, UK*
[2]*Department of Systems Biology, Harvard Medical School, 200 Longwood Avenue, Boston MA 02115, USA*
[3]*MRC Cancer Cell Unit, Hutchison-MRC Research Centre, Cambridge CB2 2XZ, UK*
[4]*Wellcome Trust/Cancer Research UK Gurdon Institute, University of Cambridge, Tennis Court Road, Cambridge CB2 1QN, UK*

Understanding how stem cells are regulated in adult tissues is a major challenge in cell biology. In the basal layer of human epidermis, clusters of almost quiescent stem cells are interspersed with proliferating and differentiating cells. Previous studies have shown that the proliferating cells follow a pattern of balanced stochastic cell fate. This behaviour enables them to maintain homeostasis, while stem cells remain confined to their quiescent clusters. Intriguingly, these clusters reappear spontaneously in culture, suggesting that they may play a functional role in stem cell auto-regulation. We propose a model of pattern formation that explains how clustering could regulate stem cell activity in homeostatic tissue through contact inhibition and stem cell aggregation.

Keywords: stem cells; pattern formation; epidermis

1. INTRODUCTION

To achieve homeostasis in adult tissues, new cells must be generated at a rate that exactly matches cell loss. Tissue maintenance is believed to depend upon long-lived stem cells, which both self-renew and generate short-lived progeny that in turn produce terminally differentiated cells [1]. Understanding how the balance between proliferation and differentiation of stem cells and their progeny is regulated to generate precisely the required number of differentiated cells is a major challenge in stem cell biology.

Mammalian epidermis is an ideal system in which to address this problem as it is constantly turned over, has a simple architecture, and is predominantly composed of a single cell lineage, the epidermal keratinocyte. The tissue is organized into hair follicles interspersed with interfollicular epidermis (IFE), which consists of layers of keratinocytes [2] (figure 1). Cells are continually shed from the surface of the IFE and replaced by proliferation in the basal cell layer. On commitment to terminal differentiation, basal cells exit the cell cycle and migrate into the suprabasal cell layers, eventually reaching the epidermal surface where they are shed. Studies in mice have revealed that, while a population of stem cells resides in the bulge of the hair follicle, these cells play no role in supporting normal IFE [3–6]. This raises the question of how homeostasis of IFE is achieved.

It has long been argued that mammalian IFE is both maintained and regenerated by stem cells, which generate a short-lived population of transit-amplifying (TA) cells that differentiate after a limited number of cell divisions [7,8]. However, this stem/TA cell paradigm has been challenged by cell fate data in transgenic mice, which revealed that murine IFE is maintained by a single population of cells that behave stochastically, dividing to generate, on average, equal numbers of cycling and post-mitotic (PM) cells [9,10]. Although, as a population, these cells exhibit the stem-like capacity for long-term self-renewal, the limited proliferative potential of individual cells led us to term them 'committed progenitor' (CP) cells [9,11,12].

The discovery of a new paradigm for tissue homeostasis in mouse IFE raises the question as to whether similar rules may govern the behaviour of keratinocytes in human epidermis. Although the general architecture of human IFE is similar to mouse, there is strong experimental evidence for proliferative heterogeneity within the basal cell layer. Sub-cloning single cell-derived colonies of cultured human keratinocytes defines distinct types of colony-initiating cells: those with a very high proliferative potential that give rise to large circular colonies when subcloned (termed holoclones); those with very limited proliferative potential that give rise to small irregularly shaped colonies (paraclones); and colonies with intermediate properties (meroclones) [13]. Subsequent studies showed that cultured keratinocytes could be fractionated on the basis of their expression of the β_1 integrin family of extracellular matrix receptors. Cells expressing high levels of β_1 integrin form large actively growing colonies and regenerate human epidermis when xenografted. In contrast, keratinocytes

*Author for correspondence (bds10@cam.ac.uk; allon@cantab.net).

Received 16 April 2011
Accepted 11 May 2011

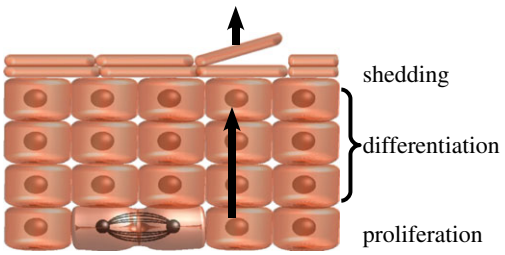

Figure 1. Schematic showing the general architecture of interfollicular epidermis (IFE). IFE is a stratified tissue in which all cell division takes place in the basal later. On commitment to terminal differentiation, cells detach from the basement membrane and move through the suprabasal cell layers, and are eventually shed. (Online version in colour.)

lower in expression form small abortive colonies in which all cells eventually undergo terminal differentiation; these cells fail to produce epidermis in xenografts [14]. Several further human epidermal stem cell markers have been defined (high expression of the notch ligand Delta, MCSP, LRIG1 and low expression of DSG3), which all co-localize with β_1 integrin [15–20]. As with β_1 integrin, the expression of these markers correlates strongly with stem cell behaviour, although their biological role in controlling stem cell fate remains unclear.

Analysis of stem cell marker expression in human IFE reveals that the basal layer is organized into irregular clusters of stem cells, localized around the tips of dermal papillae [14,15,18,20]. A striking feature of these clusters is that the great majority of the constituent cells are quiescent: proliferating cells with a much lower proliferative potential and PM basal layer cells lie between the clusters (figure 2) [15,21].

Here, we examine the cellular behaviour that underlies human epidermal homeostasis. Recently, a quantitative analysis of primary human keratinocytes has shown that CP cell behaviour is conserved even when cells are cultured at clonal density (V. Nikolaidou-Neokosmidou and P. H. Jones 2010, unpublished data). Further, this study revealed that primary human keratinocytes in three-dimensional cultures reconstitute the same pattern of stem cell clusters seen in epidermis. These results are used here to develop a theory that suggests how stem cell proliferation and differentiation may be spontaneously balanced in homeostatic tissue.

2. SPONTANEOUS STEM CELL PATTERNING

Intriguingly, when clonal density keratinocyte cultures are maintained beyond confluence (i.e. when all cells in the culture lie in contact with neighbours), stem cells are not randomly distributed within the resulting sheets of keratinocytes but are found to be clustered [14] (figure 3*a*). The organization of the basal layer in the organotypic culture is remarkably similar to epidermis (figure 2), with cells expressing the stem cell marker MCSP forming irregularly shaped clusters of similar size to those seen *in vivo*. The reconstitution of patterning, even in a hyper-proliferative culture grown on plastic in serum-free media, indicates that pattern formation is not specified by signals from other cell types,

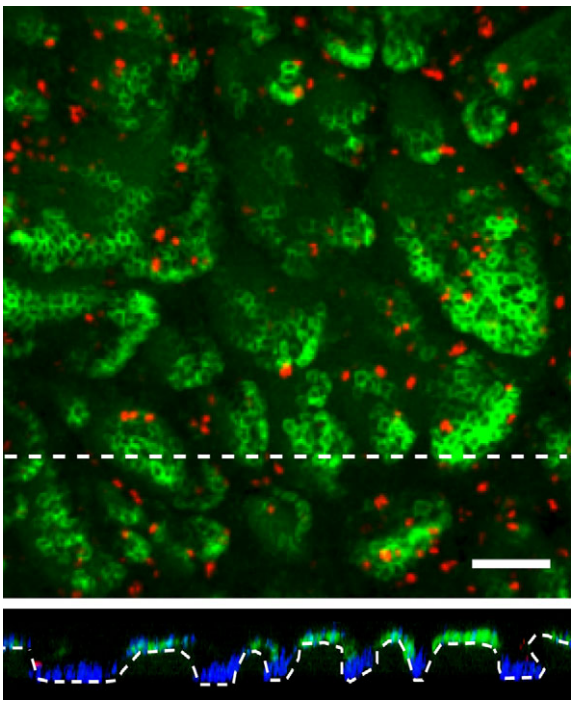

Figure 2. Rendered confocal Z-stack of whole-mounted abdominal human epidermis stained for the stem cell marker MCSP (green), the proliferation marker, Ki67 (red) and the nuclear stain DAPI (blue). Lower panel shows the basal layer in cross sections along the dashed lines. Scale bar = 100 μm. (Online version in colour.)

but is instead an intrinsic property of the keratinocytes. Moreover, the ability of the progeny of a single stem cell or multiple stem and CP cells plated at random to arrange themselves into patterned arrays indicates that patterning is a robust, spontaneous, process tuned to produce a pattern similar to that seen *in vivo* over a wide range of initial culture conditions.

How might such clustering occur, and does it offer any insight into stem cell regulation? Previously, it has been reported that stem cells adhere more tightly to each other than to other basal cells by virtue of expressing factors that promote cohesiveness, such as the notch receptor delta and MCSP [15,17]. However, although stem cell aggregation may drive rapid cluster formation, it cannot alone regulate cluster size to generate an array of small clusters [22]: this can only occur if, in addition to simple adhesion, stem cells respond to signals from adjacent cells.

3. FROM EXPERIMENTAL PHENOMENOLOGY TO THEORY

To explore the factors responsible for arresting the growth of stem cell clusters, and to gain insight into the potential functional benefits of this organization, in the following we will develop a model of epidermal maintenance that accommodates the range of experimental phenomenology. The model includes the three functionally distinct populations found in the basal layer: stem, CP and PM cells. In homeostasis, IFE is largely maintained by the turnover of the CP cell population, while stem cells retain the capacity to undergo

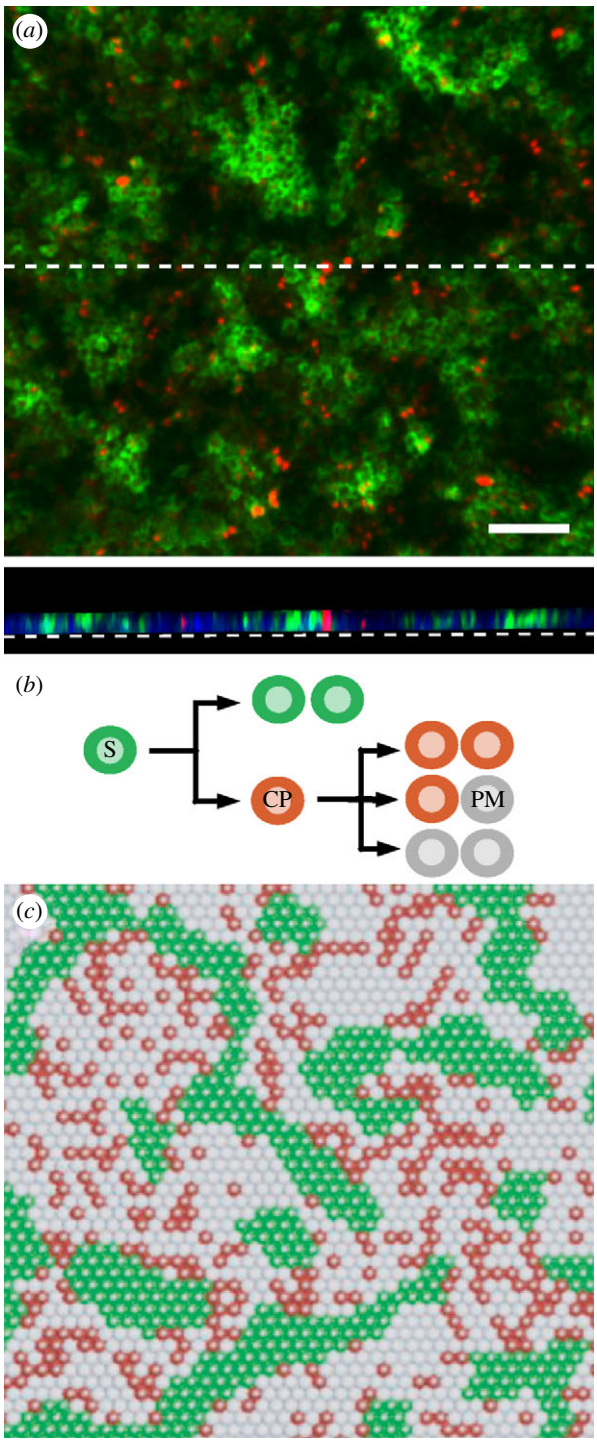

Figure 3. (*a*) Rendered confocal Z-stack of an organotypic culture of primary human keratinocytes grown on plastic, stained for the stem cell marker MCSP (green) and the marker of cell division Ki67 (red). Scale bar = 100 μm. Lower panel shows the basal layer in cross section along the dashed line, DAPI is shown in blue. (*b*) Cell lineage in the stem/CP model. Stem cells (S, green) give rise to committed progenitor cells (CP, red) that can independently maintain tissue through stochastic division giving rise to equal numbers of CP and post-mitotic (PM) cells. In addition to the lineage structure shown, the model assumes that stem cells adhere to one another, and that cell division is contact-inhibited. (*c*) Typical realization of the stem/CP cell model, obtained through a cellular automata simulation (see appendix). Cell colours correspond to the cell types in (*b*). (Online version in colour.)

division and differentiation, but remain quiescent. In the following, we will show that the patterning and turnover of IFE can be captured in full by focusing on just two stem cell fates: symmetric stem cell division leading to self-renewal, and direct differentiation of stem into CP cells in the absence of division (figure 3*b*). To incorporate stem cell cohesion into the model, we assume that stem cells effectively adhere more to each other than to other basal cells.

As PM cells exit the basal layer through upward migration, nearby cells are rearranged to ensure tissue confluence. To maintain the number of cells in the basal layer, cell loss by migration is compensated by proliferation. Therefore, in this model, we assume that cell division is regulated through a mechanism of 'contact inhibition' in which stem and CP cell division occurs only in response to the upwards migration of a nearby PM cell out of the basal layer. This constraint imposes a near-uniform cell density in the basal layer as observed experimentally. Although the model does not constrain the molecular mechanism for cell fate regulation, no further level of detail is necessary to explain the origin of pattern formation: these properties alone are already sufficient to recover patterning.

To demonstrate that this 'stem/CP cell' model can reproduce the experimental pattern, we conducted numerical simulations of the cell dynamics using a simple cellular automata (see appendix). These studies reveal that an irregularly patterned array, closely resembling that seen *in vivo*, develops from an initial random cell distribution (figure 3*c*). The patterning was found to be robust with respect to variations in the model parameters: while the quantitative characteristics of the stem cell clusters depend on the particular rates of division, differentiation and detachment from the basal layer, the pattern was consistently observed across a wide range of parameters and initial conditions. Indeed, numerical simulation shows that the same irregular patterned array can be developed from the clonal evolution of a single stem cell, as seen in experiment [14].

Although the simulations confirm that the model (figure 3*b*) has the capacity to recover the spatial organization of cells in IFE, it does not identify the actual mechanism of pattern formation, nor its importance for self-regulating the stem and CP cell populations. To address these questions, we will develop a continuum theory of the model that captures how the stem, CP and PM basal cell densities change with time within the cellular automata model. The continuum theory is heuristically constructed by including all low-order contributions of the averaged cell densities and their gradients, which are allowed by symmetry [23]. As such, the theory will capture the long-range dynamics of the cell densities, with short-range fluctuations coarse-grained out of the problem. We follow a well-established methodology for modelling non-equilibrium populations using a reaction–diffusion approach [24]. Specific examples that are closely related to the model under consideration can also be found in Lara-Ochoa [25] and Glotzer *et al.* [26]. By surrendering information about the interactions between individual cells, this theoretical approach exposes the relevant population

behaviour that leads to patterning at length scales much larger than that of a single cell.

3.1. Cahn–Hilliard equations

To discriminate between different cell types in the basal cell layer, the local cell density (defined in units of the cross-sectional area of a typical basal cell) may be subdivided into the sum, $c(\boldsymbol{r},t) = c_{\mathrm{S}}(\boldsymbol{r},t) + c_{\mathrm{A}}(\boldsymbol{r},t) + c_{\mathrm{B}}(\boldsymbol{r},t)$, of stem (S type), CP (A type) and PM (B type) cell densities. Changes in the local cell densities arising from the stem/CP behaviour (figure 3*b*) can then be expressed as a set of 'continuity' or kinetic equations for each of the three cell types, X= S, A or B,

$$\partial_t c_{\mathrm{X}} = R_{\mathrm{X}} - \nabla \cdot \boldsymbol{J}_{\mathrm{X}}\,. \tag{3.1}$$

Processes that change the total number of cells of each type appear as rates, R_{X}, which incorporate the average rates of cell division, differentiation and upward migration. At the same time, changes to the local cell densities may also result from the rearrangement of cells within the basal layer. The resulting redistribution of cell densities is associated with a flow of cells, or flux, $\boldsymbol{J}_{\mathrm{X}}$. The processes of cell division and differentiation in the stem/CP cell model (figure 3*b*) can be related to the rates,

$$\left.\begin{aligned} R_{\mathrm{S}} &= (\gamma_{\mathrm{SS}}^{(\mathrm{S})} - \gamma_{\mathrm{A}}^{(\mathrm{S})})c_{\mathrm{S}}, \\ R_{\mathrm{A}} &= \gamma_{\mathrm{A}}^{(\mathrm{S})} c_{\mathrm{S}} - \Delta c_{\mathrm{A}} \\ \text{and} \qquad R_{\mathrm{B}} &= \Gamma c_{\mathrm{A}} - \gamma^{(\mathrm{B})} c_{\mathrm{B}}, \end{aligned}\right\} \tag{3.2}$$

where $\gamma_{\mathrm{YZ}}^{(\mathrm{X})}$ is the average division rate of cell type X into two daughter cells (type Y, Z). $\gamma_{\mathrm{A}}^{(\mathrm{S})}$ denotes the differentiation rate of stem cells into CP cells, $\Delta = \gamma_{\mathrm{BB}}^{(\mathrm{A})} - \gamma_{\mathrm{AA}}^{(\mathrm{A})}$ is the effective differentiation rate of CP cells into PM cells, $\Gamma = 2\gamma_{\mathrm{BB}}^{(\mathrm{A})} + \gamma_{\mathrm{AB}}^{(\mathrm{A})}$ is the net rate at which CP cells generate PM cells and $\gamma^{(\mathrm{B})}$ is the rate of migration (i.e. exit) of PM cells from the basal layer. During homeostasis, the cell division rates are regulated by the local cell density with the cell division rates vanishing at the saturating cell density, c_0, imposed by contact inhibition. As the steady-state cell density will be very close to c_0, the cell division rates are dominated by a leading-order density dependence, which is taken to be linear, viz. $\gamma_{\mathrm{YZ}}^{(\mathrm{X})}(\boldsymbol{r},t) = (1 - c(\boldsymbol{r},t)/c_0) r_{\mathrm{YZ}}^{(\mathrm{X})}$, and therefore $\Gamma(\boldsymbol{r},t) = (1 - c(\boldsymbol{r},t)/c_0) r_\Gamma$, $\Delta(\boldsymbol{r},t) = (1 - c(\boldsymbol{r},t)/c_0) r_\Delta$. As defined above, $c(\boldsymbol{r},t) \le c_0$ is the total local cell density, $r_{\mathrm{YZ}}^{(\mathrm{X})}$ denotes the constant bare division rates, and $r_\Gamma = 2r_{\mathrm{BB}}^{(\mathrm{A})} + r_{\mathrm{AB}}^{(\mathrm{A})}$, $r_\Delta = r_{\mathrm{BB}}^{(\mathrm{A})} - r_{\mathrm{AA}}^{(\mathrm{A})}$ follow the same definitions as Γ and Δ. Higher-order corrections will contribute little to the steady-state behaviour. In units of the cross-section area of the cells, the saturating density is $c_0 = 1$.

We now turn to the effects of cell rearrangement and stem cell adhesion. If the reaction terms R_{X} were absent and cells were allowed to migrate in the basal layer, the adhesion of stem cells would lead them to 'phase separate' according to a mean-field flux first described by Cahn & Hilliard [27]. For our system, we can follow the same approach to modelling the cell flux despite the presence of reaction terms and absence of active cell migration, by defining a free-energy functional $F[\{c_{\mathrm{X}}\}]$ that concisely captures the effect of all local forces acting on the cells, as well as diffusive effects that arise from the stochastic nature of cell division. Defining the mobility matrix M_{XY}, the flux in the density of cell type X is given by

$$\mathbf{J}_{\mathrm{X}} = -\sum_{\mathrm{Y}\in\{\mathrm{S,A,B}\}} M_{\mathrm{XY}} \nabla\left(\frac{\delta F}{\delta c_{\mathrm{Y}}}\right), \tag{3.3}$$

where $(\delta F/\delta c_{\mathrm{Y}})$ is the functional derivative of the free energy, which acts as a local 'chemical potential' of cell type Y such that cells move from regions of high to low chemical potential. The confluence and near-uniform density of the basal layer suggest the use of a mobility matrix of Onsager-type (i.e. 'hard-core' particles). This form of M_{XY} explicitly ensures that cell rearrangements do not change the overall cell density (i.e. $\sum_{\mathrm{Y}} M_{\mathrm{XY}} = 0$) — a cell can only move if other neighbouring cells move concurrently to ensure no 'gaps' form. For simplicity, we assume that all cells have similar rates of migration at confluence, such that the mobility matrix is characterized by a single diffusion constant, σ. Referring to Elliott & Garcke [28], the relevant form of the mobility matrix is given by $M_{\mathrm{XY}} = \sigma c_{\mathrm{X}}(\delta_{\mathrm{XY}} - c_{\mathrm{Y}}/c_0)$.

To identify the relevant free energy $F[\{c_{\mathrm{X}}\}]$, one must account for the dominant processes that lead to a cell flux in a confluent tissue. We consider three processes:

— *Cell rearrangement following cell exit or mitosis.* As PM cells exit the basal layer, neighbouring cells occupy their basal layer footprint through division and rearrangement. We shall model the effect of cell motion on the cell densities, c_{X}, through simple diffusion on two timescales: at times that are fast comparable to the rate of cell division and differentiation, cell rearrangement ensures that the overall cell density, $c = \sum_{\mathrm{X}} c_{\mathrm{X}}$, remains uniform. At long times, the three cell types (stem, CP and PM) become mixed through ongoing rearrangement leading to a slow diffusion of the areal fractions of the different cells types. The fast and slow processes are captured by an effective free energy that resembles an entropy of mixing [27], viz.

$$F_0 = \int d^2 r \left[\sum_{\mathrm{X}} c_{\mathrm{X}} \ln c_{\mathrm{X}} + \chi(1-c)\ln(1-c)\right],$$

where the 'slow' diffusion constant is given by the mobility σ (defined above), and the constant $\chi \gg 1$ gives the ratio between the fast and slow diffusion timescales.

— *Stem cell adhesion.* The effect of adhesion is similar to that of surface tension in phase-separating mixtures. Drawing upon the long history of literature in this field, we will use the Cahn–Hilliard free energy [27] that was first used to study phase separation,

$$F_{\mathrm{adh.}} = -\frac{J}{2}\int d^2 r \left[c_{\mathrm{S}}^2 - \frac{1}{2}\alpha(\nabla c_{\mathrm{S}})^2\right].$$

Here, the parameter J gives the strength of stem cell adhesion relative to diffusion, while α is a constant of order unity (commonly known as the 'surface tension')

that depends on the geometrical arrangement of cells within the basal layer.

— *Density diffusion owing to stochastic cell fate.* The stochastic outcome of CP cell division leads to an effective diffusion of CP and PM cells [29]. For example, consider the outcome of asymmetric CP cell division, $A \rightarrow A + B$: following division, the position of the daughter CP cell may be displaced from that of the parent CP cell by perhaps half a cell diameter. As a result, a sequence of asymmetric divisions will translate into an effective random walk for the CP cell progeny. Likewise, the balance of symmetric division and differentiation leads to diffusion of the average local cell density, see [29]. Together, the magnitude of the diffusion constant resulting from stochastic cell division is set by the CP cell division rate, Γ/c_0 [29]. However, we may absorb this diffusion entirely into the first term of the free energy, F_0.

Finally, as uninjured epidermis has no open edges, the appropriate boundary conditions for equation (3.1) are periodic. In practice, for much of the following analysis we may treat the basal layer as an infinite two-dimensional surface and neglect boundary conditions. For exact numerical solutions of equation (3.1), however, we impose the periodic boundary conditions.

3.2. Parameter timescales

The tissue biology presents several constraints on the timescales of the model parameters (table 1). Based on the analysis of cell division rates in mouse epidermis [9,10], which is expected to be close to human, PM cells exit the basal layer with a rate of $\gamma^{(B)} \approx 0.3 - 1/\text{week}$, and cycling CP cells divide with a rate of $\Gamma = r_\Gamma(1 - c/c_0) \approx 1/\text{week}$. As diffusion of the cell density is driven by the same two processes of CP cell division and PM cell exit, it follows that $\sigma \sim (\gamma^{(B)} + \Gamma)/c_0$. Turning to the stem cells, their quiescence and rare differentiation set the slowest timescales in the system to be the stem cell differentiation rate, $\gamma^{(S)}/\gamma^{(B)} \ll 1$, their division rate, $\gamma_{SS}^{(S)}/\Gamma \ll 1$ and the CP cell loss rate, $\Delta/\Gamma \ll 1$.

In addition, stem cells, cycling progenitors and PM cells are present in comparable fractions in the basal layer (estimated in the range 20–40% [13]), which imposes two additional parameter constraints, while the size of the stem cell clusters (approx. 14 cells in diameter [14,21]) imposes yet a third additional constraint. To determine the dependence of these observables on the model parameters, it is necessary to analyse equation (3.1) to identify properties of the steady-state pattern. In the following analysis, we will work in units of the cell area $c_0 = 1$.

3.3. Stability and pattern formation

As well as the trivial fixed points of the empty ($c = 0$), and 'jammed' ($c = c_A = 1$)[1] systems, the kinetic equation (3.1) admits a uniform steady-state solution

[1]Although the 'jammed' fixed point is unphysiological, it is generically unstable with respect to density fluctuations. It is therefore irrelevant when focussing on density configurations far from the jammed fixed point.

Table 1. Overview of mean-field model parameters.

$\gamma_{SS}^{(S)}$	stem cell division rate
$\gamma_A^{(S)}$	stem cell differentiation rate into CP (type A) cells
Δ	loss rate of CP cells
Γ	birth rate of post-mitotic (type B) cells
$\gamma^{(B)}$	basal layer exit rate of post-mitotic cells
c_0	cell areal density (=1 cell per unit area)
σ	effective cell mobility
χ	ratio of elastic (fast) diffusion to mixing (slow) diffusion
J	strength of stem cell adhesion
α	surface tension of stem cell adhesion
$r_{SS}^{(S)}$, r_Δ, r_Γ	'bare' division rates (linear coefficients of rate density dependencies)

with $\bar{c}_A = (r_{SS}^{(S)}/r_\Delta)\bar{c}_S$, $\bar{c}_B = (r_\Gamma \gamma_A^{(S)}/r_\Delta \gamma^{(B)})\bar{c}_S$ and $\bar{c} = \bar{c}_S + \bar{c}_A + \bar{c}_B = 1 - \gamma_A^{(S)}/r_{SS}^{(S)}$. (Recall that we have set $c_0 = 1$, and that the rates r_X relate to the bare reaction rates, undressed by the excluded volume factor, $(1 - c(\boldsymbol{r}, t))$.) Linearizing the kinetic equations in fluctuations $\delta c_X \propto e^{\nu(\mathbf{k})t + i\mathbf{k}\cdot\mathbf{r}}$, one obtains an eigenvalue equation for the growth rate of modes $\mathbf{k}$. Although the formal analytical expressions for the eigenvalues, $\nu(\mathbf{k})$, are unwieldy, the stability properties can be easily inferred for the physical system. In particular, for $\mathbf{k}$ large, the stability behaviour is dictated by the adhesion properties of the stem cell compartment alone. As a result, one finds that $\nu(\mathbf{k}) \simeq \sigma\mathbf{k}^2[J\bar{c}_S(1-\bar{c}_S)(1-\alpha\mathbf{k}^2)\mathbf{k}^2 - 1]$ with the most unstable mode set by

$$k_{\max} \simeq \frac{J\bar{c}_S(1-\bar{c}_S) - 1}{2\alpha J\bar{c}_S(1-\bar{c}_S)}.$$

However, for small $\mathbf{k}$, the stability properties are instead dictated by division/differentiation where the fixed point is stable (figure 4*a*).

Such a crossover between reaction-induced stability and adhesion-induced instability appears to be typical for systems involving both reactions and spinodal decomposition [25,26]. Referring to the phase-space dynamics in figure 4*b*, one may qualitatively interpret the behaviour as follows: the adhesiveness of stem cells always favours instability at short wavelengths, which leads to spinodal decomposition (thick grey arrows). However, the division/differentiation of cells has the effect of restoring the local cell populations back to their equilibrium values (dashed lines). Stability is achieved at large wavelengths, as here the stem cell aggregation driving the instability is sufficiently weak to be completely balanced out by the restoring effect of cell division and differentiation (figure 4*a*, inset). These opposing behaviours at short and long wavelengths are also responsible for arresting the coarsening as the instability matures.

Although the linear stability analysis describes the onset of the transition from a uniform to a patterned state, it says little about the morphology of the steady state. From the numerical solution for the reaction–diffusion equations (3.1), shown in figure 5, one may see that the steady state involves a near phase-

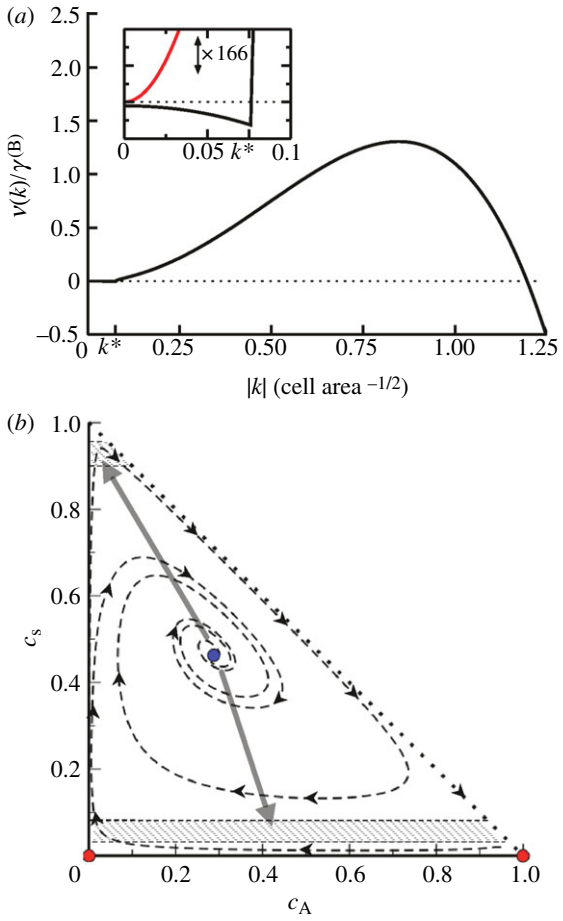

Figure 4. (*a*) Dispersion relation for the response of the system to fluctuations about the fixed point, showing stability at small wavenumbers k and spinodal-like instability at larger values of k. Inset: focus on the short wavenumber region of the dispersion relation, with vertical axis magnified ×166. The system shows a weak stable response at long wavelengths, in contrast to the case when reactions are turned off (red curve). The wavenumber k^* indicates the crossover to reactionless behaviour, setting the length scale at which the pattern is stable; $1/k^* \sim 10 - 20$ cells is consistent with the stem cell cluster size observed in experiment [14,21]. Parameters used for plotting: $r_\Gamma = 200$, $r_\Delta = 2$, $\gamma_A^{(S)} = 0.02$, $r_{SS}^{(S)} = 4$, $\sigma = 2$, $J = 12$, $\alpha = 0.33$. (*b*) The state diagram for the homogeneous-density solution to equation (3.1), projected onto the (c_S, c_A) plane. The system exhibits two unstable fixed points (red) and one stable fixed point (blue). Spatial fluctuations induce phase separation (grey arrows) into the metastable regions (hashed), which are themselves incapable of sustaining an extended homogeneous domain. (Online version in colour.)

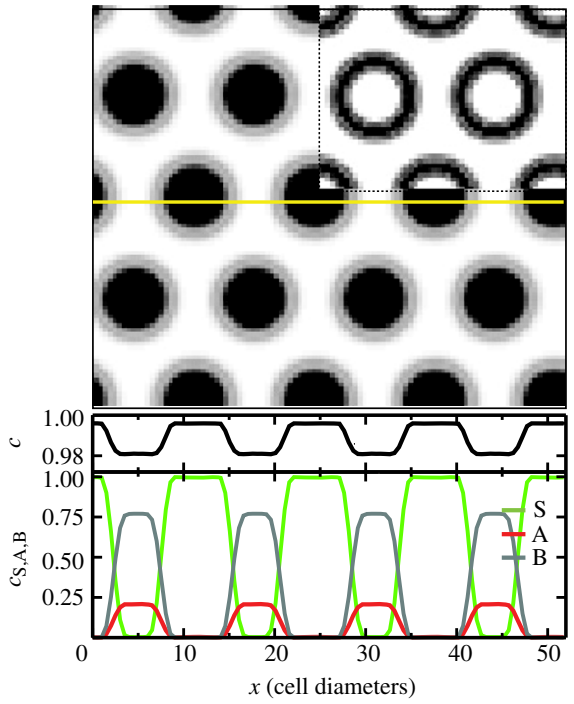

Figure 5. Predicted steady-state distribution of stem cells in the basal layer obtained from the kinetic theory (3.1). Stem cells aggregate into a periodic array of clusters (black), within a sea of committed progenitor and PM cells (white). The regularity of the pattern is due to the 'mean-field' character of the theory, which describes the average behaviour of the population. The location of dividing stem cells (with $\gamma_{SS}^{(S)} > 0$) is shown inset for the same stationary state (black), revealing that stem cells deep within each cluster are quiescent. The lower panels show the total cell density c, and the density of stem (type S), committed progenitor (type A) and PM (type B) cells along the marked cross section (yellow). Parameters used for this calculation are $\sigma = 2$, $J = 12$, $\alpha = 0.33$, $\chi = 1$, $r_\Gamma = 200$, $\gamma_{SS}^{(A)}/r_\Gamma = 0.02$, $r_\Delta/r_\Gamma = 0.01$, $\gamma^{(B)} = 1$ and $\gamma_A^{(S)} = 0.01$. (Online version in colour.)

separated periodic structure of hexagonal lattice symmetry and wavelength L. Within each lattice period, the system separates into a homogeneous circular stem cell-rich domain of area a_S and density $\bar{c}_S \simeq 1$, and a stem cell-depleted region of relative area $a_{AB} = L^2 - a_S$ and density $\bar{c}_S \simeq 1$, i.e. in the steady state, stem cell proliferation is limited to the boundary region around the stem cell-rich clusters (as seen directly in figure 5).

To maintain each stem cell-rich domain at its steady-state size, the rate of stem cell differentiation within the domain is matched by stem cell creation at the domain wall. Since we assume that stem cell adhesion is strong, $J \gg 1$, then the width, W, of the domain wall is controlled only by the adhesion properties of stem cells, with $W \propto \sqrt{\alpha}$ [30]. As a result, one obtains a natural condition for the total density $\bar{c}$ inside the stem cell-*depleted* domain,

$$W\sqrt{a_S}\,\Omega r_{SS}^{(S)}(1-\bar{c}) = a_S \gamma_A^{(S)}, \tag{3.4}$$

where $\Omega = 2\sqrt{\pi}/W \int_W \mathrm{d}r\; c_S(r)[1 - c_S(r)]$ is a dimensionless number of order unity, with the integral $\int_W \mathrm{d}r$ taken along a path perpendicular to the domain wall. Similarly, integrating equation (3.1) over the near-uniform stem cell-depleted region up to the domain wall, one obtains the following relations for the remaining effective transition rates,

$$a_{AB} r_\Delta \bar{c}_A(1-\bar{c}) \simeq a_S \gamma_A^{(S)}$$

and

$$r_\Gamma\, \bar{c}_A(1-\bar{c}) \simeq \gamma^{(B)} \bar{c}_B, \tag{3.5}$$

where $\bar{c}_A$ and $\bar{c}_B$ ($\bar{c} = \bar{c}_A + \bar{c}_B$) denote the (constant)

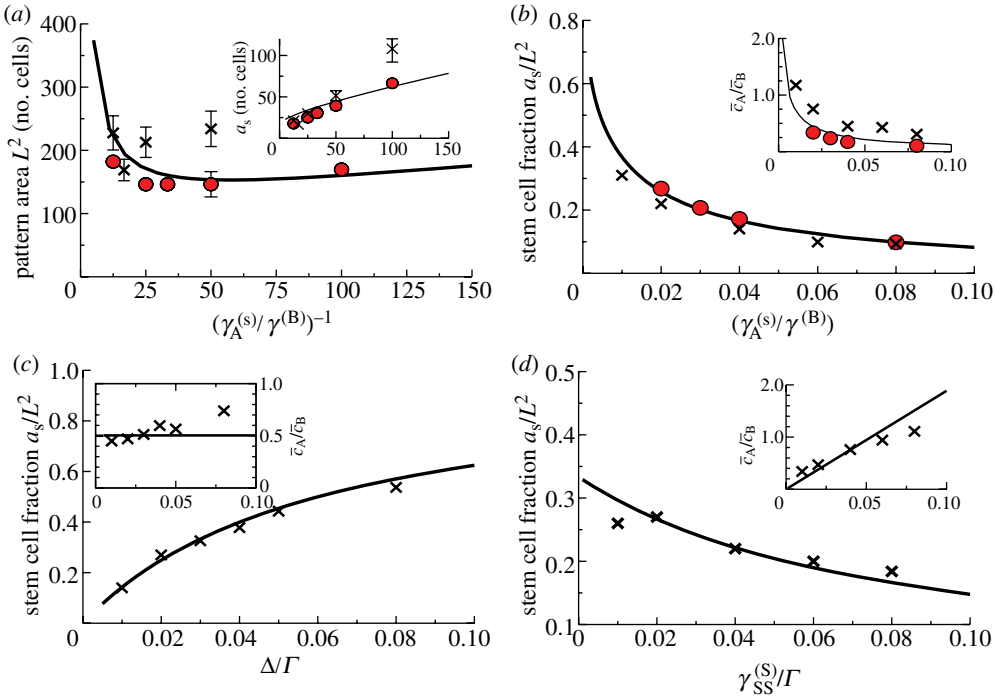

Figure 6. Parameter dependence of the patterned steady-state morphology, demonstrated by plotting the parameter dependence of (*a*) the pattern area L^2; (*a*, inset) the mean stem cell cluster size a_S; (*b*–*d*) the stem cell fraction a_S/L^2 and (*b*–*d*, insets) the ratio of CP to PM cells $\bar{c}_A/\bar{c}_B$. The solid curves correspond to the analytical approximations given by equations (3.4)–(3.6). The solid data points (red) were obtained from the numerical solution to the system equations (3.1). Error bars in (*a*) indicate the tolerance of the system to variations in the pattern wavelength, as estimated by varying the initial conditions and then testing the stability of the patterned state. The crosses (×) indicate the results obtained from cellular automata simulations of the stem/CP model that is capable of accounting for the effects of fluctuations. For the simulations, a_S was calculated as the mean size of stem cell clusters, and the length scale of the pattern, L^2, was calculated from the by dividing a_S by the steady-state fraction of stem cells in the simulation. The plots correspond to the parameter sets given in figure 4, $\gamma_A^{(S)} = 0.01$, $r_{SS}^{(S)}/r_\Gamma = 0.02$, $r_\Delta/r_\Gamma = 0.01$, and $\sigma = 4$. The pattern morphology and characteristics are largely insensitive to the precise values of J, r_Γ and α, provided that J and r_Γ are much greater than unity, and $\alpha \sim O(1)$. We used the values $J = 12$, $r_\Gamma = 200$ and $\alpha = 0.33$. Here, all lengths are measured in units of the cell diameter, and all times are measured in units of the PM cell migration time, $1/\gamma^{(B)}$. The values of W and Ω in the analytical solution were estimated by a best fit to the simulation results to be $W = 2.5$, $\Omega = 1.5$. (Online version in colour.)

densities of progenitor and PM cells inside the stem cell-depleted domain.

To estimate the size of the stem cell-rich domains, we note that the dynamics within the stem cell-rich regions are dominated by the processes of stem cell differentiation and diffusion. From dimensional analysis, we therefore expect the growth of the stem cell-rich domains to be arrested at a typical size of $a_S \propto \sigma/\gamma_A^{(S)}$, which is the size when the type A cells created within the domain begin to destabilize the domain. Taking into account the finite width W of the cluster boundary, we obtain the estimate

$$a_S \simeq A\frac{\sigma}{\gamma_A^{(S)}} + W\left(\left(\frac{A\sigma}{\gamma_A^{(S)}}\right)^{1/2} + \frac{W}{2}\right), \qquad (3.6)$$

where A is a numerical constant.

Taken together, equations (3.4)–(3.6) characterize key features of the steady-state morphology, giving access to the stem cell cluster size, the periodicity of the pattern $L^2 = a_S + a_{AB}$, as well as the fraction of progenitor cells and PM cells in the stem cell-depleted regions ($\bar{c}_A$, $\bar{c}_B$), as shown in figure 6. For example, a reduction in the ratio $\gamma_A^{(S)}\Gamma/\Delta\gamma^{(B)} \simeq a_{AB}/a_S + \mathcal{O}[a_S^{-1/2}]$ has the capacity to invert the steady-state pattern (i.e. $a_S/L^2 > 1/2$) leading to the formation of a lattice of stem cell-depleted domains within a sea of stem cells.

Finally, it is interesting to assess the effect of fluctuations on the solution to the mean-field equations. Many of the fluctuations relevant to the cellular system are captured by the cellular automata simulations (figure 3*c* and appendix), which incorporate the stochastic nature of cell fate decisions (figure 3*b*), as well as Poisson (or 'shot') noise in the chemical reactions. A comparison of the simulation results with the mean-field equations in figure 6 shows that the effect of fluctuations is most pronounced in setting the patterning length scale (figure 6*a*), which deviates strongly from the mean-field results. Fluctuations also weakly affect the ratio of CP and PM cells (figure 6*c*,*d*, insets). However, the fraction of stem cells in the basal layer (a_S/L^2) remains largely unaffected (figure 6*c*,*d*).

4. DISCUSSION

The best-known examples of pattern formation in biological systems belong to the class of Turing instabilities, whereby two chemical species, acting as an activator and inhibitor, undergo spontaneous patterning

[31]. Intriguingly, the structure of the coarse-grained equations reveals that pattern formation in the proposed model does not derive from a Turing instability, but from a process of 'surface tension'-mediated separation of the stem and non-stem cells, which results from the aggregation of stem cells (cf. [26]). Small clusters form through the combined effects of stem cell adhesion and proliferation; yet, when clusters become too large they fragment as a result of stem cell differentiation. The average diameter of the stem cell-rich clusters varies over a wide range of parameters in a predictable way, reflecting the typical cluster size at which the generation rate of CP cells through stem cell differentiation within a cluster begins to exceed the rate at which they exit the cluster into the surrounding tissue. Stem cells on the boundary of clusters should divide slowly, while contact inhibition leads to an almost complete suppression of stem cell division deep within the clusters (figure 5*a*, inset), consistent with experiment. In summary, these results show that the observed aggregation of stem cells, combined with contact inhibition, is sufficient to explain the large-scale stem cell patterning.

To assess whether patterning in human IFE provides some functional advantage, we reanalysed the stem/CP cell model to explore the importance of stem cell adhesion. In the absence of adhesion, stem cells become dispersed through tissue and, through the resulting reduction in contact inhibition, the entire stem cell population enters into cycle. This result shows that patterning could provide an effective mechanism to maintain stem cell quiescence during homeostasis: epidermal homeostasis proceeds predominantly through the turnover of CP cells, with only a small contribution arising from the differentiation and turnover of the stem cell compartment. This presents a clear functional advantage in protecting stem cells against damage. Conversely, when tissue becomes sub-confluent through wounding, the model predicts that the loss of contact inhibition leads to the rapid recruitment of the stem cell population back into cycle until the patterning is recovered and homeostasis is restored. Therefore, the proposed patterning mechanism can not only ensure stem cell quiescence, but also allows stem cells to rapidly and spontaneously switch between response to injury and homeostasis.

For many years it has been argued that long-lived, self-renewing stem cells both maintain adult tissues and regenerate them after injury. Following this concept, it was assumed that epidermal maintenance must depend on cells that generate large actively growing colonies *in vitro* and reconstitute epidermis in xenografts [13,14]. By contrast, the results presented here are consistent with human IFE being maintained not by stem cells, but by progenitor cells that only generate small or microscopic colonies in culture and lack the ability to regenerate epidermis in xenograft assays: these progenitor cells are stochastic CP cells that have a capacity for long-term self-renewal as a population, while individual CP cells typically have only a limited proliferative and self-renewal potential. CP cells maintain the tissue but are unable to regenerate it.

By contrast, stem cells have a high proliferative and self-renewal potential, evidenced by their ability to found large actively growing colonies in culture and regenerate epidermis on transplantation. Unlike CP cells, their fate is highly regulated by the environment: exponential stem cell growth in clonal culture turns to quiescence when the epidermis is reconstituted. Moreover, stem cells cohere while CP cells are distributed randomly in the IFE. By combining these experimental observations with the properties of CP cells, the stem/CP cell model suggests that the full gamut of reported human IFE stem cell behaviour might be explained by a simple theory (figure 3*b*). We suggest that patterning is a mechanism of stem cell auto-regulation; mutual adhesion leads to stem cell cluster formation that, through contact inhibition, drives the stem cells into quiescence. Thus, rather than being regulated by signals from other cell types within a niche, human IFE stem cells assemble themselves into quiescent clusters. The simple rules of stem and CP cell behaviour create an environment that achieves the same regulation that the niche confers on stem cells in other lineages.

P.H.J. is supported by the MRC and B.D.S. acknowledges the financial support of the MRC and EPSRC.

APPENDIX A. CELLULAR AUTOMATA SIMULATIONS

To develop a cell-based model that incorporates many of the features of a stochastic cell population, we adopt the approach described in Kein *et al.* [32]. We model the basal layer as a two-dimensional (hexagonal) lattice where each site may host one of the three cell types or may be vacant (⊘). To further maintain a uniform cell density through density-dependent cell division rates, we suppose that progenitor cells are only capable of division when neighbouring a vacancy. Thus, the symmetric and asymmetric divisions of the CP cell compartment and the migration of PM cells from the basal layer may be summarized by the processes

$$\mathrm{A}\oslash \rightarrow \begin{cases} \mathrm{A} & \mathrm{A} & r^{(\mathrm{A})}_{\mathrm{AA}}/z \\ \mathrm{A} & \mathrm{B} & r^{(\mathrm{A})}_{\mathrm{AB}}/z, \\ \mathrm{B} & \mathrm{B} & r^{(\mathrm{A})}_{\mathrm{BB}}/z \end{cases} \qquad \mathrm{B} \overset{\gamma^{(\mathrm{B})}}{\rightarrow} \oslash.$$

The parameters $r^{(\mathrm{X})}_{\mathrm{YZ}}$ represent the respective 'reaction' rates, which are related to the coarse-grained parameters through the identities $r_{\Gamma} = r^{(\mathrm{A})}_{\mathrm{AB}} + 2r^{(\mathrm{A})}_{\mathrm{BB}}$, and $r_{\Delta} = r^{(\mathrm{A})}_{\mathrm{BB}} - r^{(\mathrm{A})}_{\mathrm{AA}}$, and $z = 6$ denotes the coordination number of the lattice. To accommodate the process of lateral cell mobility, we include the 'fast' vacancy diffusion process, $\mathrm{X}\oslash \overset{\chi'}{\rightarrow} \oslash\mathrm{X}$, where X = A,B, and the hopping rate $\chi' \propto \chi\sigma$ is related to the coarse-grained mobility, σ, (in units of the cell area) and to the 'fast' timescale of the elastic tissue response, χ, through a constant numerical factor of order unity, (for example, $\chi' = \frac{2}{3}\chi\sigma$ for a hexagonal lattice).

Without stem cells, when $\gamma^{(\mathrm{A})}_{\mathrm{AA}} = \gamma^{(\mathrm{A})}_{\mathrm{BB}}$, the model above describes a critical birth–death process belonging to the generalized Voter universality class [29]. Turning to the stem cell compartment, and allowing for symmetric stem cell division or differentiation, the lattice

model is related to the coarse-grained model through the processes

$$\mathrm{S}\oslash \overset{r_{\mathrm{SS}}^{(\mathrm{S})}/z}{\rightarrow} \mathrm{S\,S} \text{ and } \mathrm{S} \overset{\gamma_{A}^{(\mathrm{S})}}{\rightarrow} \mathrm{A}. \tag{A 1}$$

Finally, turning to the processes of stem cell mobility and clustering, there does not exist (to our knowledge) any microscopic model for which the Cahn–Hilliard dynamics of equation (3.1) gives the exact macroscopic description [33]. Nevertheless, the same qualitative behaviour (and much of the quantitative behaviour) is captured by the constrained diffusion processes

$$\mathrm{S}_i\mathrm{X}_j \overset{w_{ij}}{\rightarrow} \mathrm{X}_i\mathrm{S}_j \quad \text{and} \quad \mathrm{S}_i\oslash_j \overset{\chi w_{ij}}{\rightarrow} \oslash_i \mathrm{S}_j, \tag{A 2}$$

with the exchange rate w_{ij} reflecting the change in energy from the initial to the target states. We define the exchange rate using Glauber's hyperbolic tangent rule, $w_{ij} = \sigma'(1 - \tanh[E_j - E_i - J])/2$, where $E_i = J\sum_{k\in \mathrm{N}(i)} n_{\mathrm{S},k}$ is the relative energy of the system when the stem cell is at its initial site i, E_j is the energy evaluated when the stem cell has hopped to its neighbouring site and $\mathrm{N}(i)$ denotes the neighbours of lattice site i and $n_{\mathrm{S},k} \in \{0,1\}$ is the stem cell occupancy at site k (other functional forms of E_i give similar results). With respect to stem cell motion, this model is the dynamic Ising model with conserved particle number—the Kawasaki model [34].

To implement the basal layer lattice simulation, we used a Gillespie algorithm [35], treating all processes as Poisson. Using this algorithm, the system was allowed to evolve over a time $t \gg \gamma_{\mathrm{A}}^{(\mathrm{S})}$ until a steady state was reached, as determined by requiring that the average fraction of cells of type $\mathrm{X} \in \mathrm{S}$, A and B become stationary. By varying the choice of system parameters, it was possible to study the nature of the steady state associated with the microscopic model.

REFERENCES

1 Lajtha, L. G. 1979 Stem cell concepts. *Differentiation* **14**, 23–34. (doi:10.1111/j.1432-0436.1979.tb01007.x)

2 Fuchs, E. 2007 Scratching the surface of skin development. *Nature* **445**, 834–842. (doi:10.1038/nature05659)

3 Tumbar, T., Guasch, G., Greco, V., Blanpain, C., Lowry, W. E., Rendl, M. & Fuchs, E. 2004 Defining the epithelial stem cell niche in skin. *Science* **303**, 359–363. (doi:10.1126/science.1092436)

4 Claudinot, S., Nicolas, M., Oshima, H., Rochat, A. & Barrandon, Y. 2005 Long-term renewal of hair follicles from clonogenic multipotent stem cells. *Proc. Natl Acad. Sci. USA* **102**, 14 677–14 682. (doi:10.1073/pnas.0507250102)

5 Levy, V., Lindon, C., Harfe, B. D. & Morgan, B. A. 2005 Distinct stem cell populations regenerate the follicle and interfollicular epidermis. *Dev. Cell* **9**, 855–861. (doi:10.1016/j.devcel.2005.11.003)

6 Ito, M., Liu, Y., Yang, Z., Nguyen, J., Liang, F., Morris, R. J. & Cotsarelis, G. 2005 Stem cells in the hair follicle bulge contribute to wound repair but not to homeostasis of the epidermis. *Nat. Med.* **11**, 1351–1354. (doi:10.1038/nm1328)

7 Mackenzie, I. C. 1970 Relationship between mitosis and the ordered structure of the stratum corneum in mouse epidermis. *Nature* **226**, 653–655. (doi:10.1038/226653a0)

8 Potten, C. S. 1974 The epidermal proliferative unit: the possible role of the central basal cell. *Cell Tissue Kinet.* **7**, 77–88.

9 Clayton, E., Doupé, D. P., Klein, A. M., Winton, D. J., Simons, B. D. & Jones, P. H. 2007 A single type of progenitor cell maintains normal epidermis. *Nature* **446**, 185–189. (doi:10.1038/nature05574)

10 Doupé, D. P., Klein, A. M., Simons, B. D. & Jones, P. H. 2010 The ordered architecture of murine ear epidermis is maintained by progenitor cells with random fate. *Dev. Cell* **18**, 317–323. (doi:10.1016/j.devcel.2009.12.016)

11 Jones, P. H., Simons, B. D. & Watt, F. M. 2007 Sic transit gloria: farewell to the epidermal transit amplifying cell? *Cell Stem Cell* **1**, 371–381. (doi:10.1016/j.stem.2007.09.014)

12 Jones, P. H. & Simons, B. D. 2008 Epidermal homeostasis: do committed progenitors work while stem cells sleep? *Nat. Rev. Mol. Cell Biol.* **9**, 82–88. (doi:10.1038/nrm2292)

13 Barrandon, Y. & Green, H. 1987 Three clonal types of keratinocyte with different capacities for multiplication. *Proc. Natl Acad. Sci. USA* **84**, 2302–2306. (doi:10.1073/pnas.84.8.2302)

14 Jones, P. H., Harper, S. & Watt, F. M. 1995 Stem cell patterning and fate in human epidermis. *Cell* **80**, 83–93. (doi:10.1016/0092-8674(95)90453-0)

15 Legg, J., Jensen, U. B., Broad, S., Leigh, I. & Watt, F. M. 2003 Role of melanoma chondroitin sulphate proteoglycan in patterning stem cells in human interfollicular epidermis. *Development* **130**, 6049–6063. (doi:10.1242/dev.00837)

16 Lowell, S. & Watt, F. M. 2001 Delta regulates keratinocyte spreading and motility independently of differentiation. *Mech. Dev.* **107**, 133–140. (doi:10.1016/S0925-4773(01)00459-2)

17 Estrach, S., Legg, J. & Watt, F. M. 2007 Syntenin mediates Delta1-induced cohesiveness of epidermal stem cells in culture. *J. Cell Sci.* **120**, 2944–2952. (doi:10.1242/jcs.016253)

18 Jensen, K. B. & Watt, F. M. 2006 Single-cell expression profiling of human epidermal stem and transit-amplifying cells: Lrig1 is a regulator of stem cell quiescence. *Proc. Natl Acad. Sci. USA* **103**, 11 958–11 963. (doi:10.1073/pnas.0601886103)

19 Wan, H., Stone, M. G., Simpson, C., Reynolds, L. E., Marshall, J. F., Hart, I. R., Hodivala-Dilke, K. M. & Eady, R. A. 2003 Desmosomal proteins, including desmoglein 3, serve as novel negative markers for epidermal stem cell-containing population of keratinocytes. *J. Cell Sci.* **116**, 4239–4248. (doi:10.1242/jcs.00701)

20 Wan, H., Yuan, M., Simpson, C., Allen, K., Gavins, F. N. E., Ikram, M. S., Basu, S., Baksh, N., O'Toole, E. A. & Hart, I. R. 2007 Stem/progenitor cell-like properties of desmoglein 3dim cells in primary and immortalized keratinocyte lines. *Stem Cells* **25**, 1286–1297. (doi:10.1634/stemcells.2006-0304)

21 Jensen, U. B., Lowell, S. & Watt, F. M. 1999 The spatial relationship between stem cells and their progeny in the basal layer of human epidermis: a new view based on whole-mount labelling and lineage analysis. *Development* **126**, 2409–2418.

22 Savill, N. J. & Sherratt, J. A. 2003 Control of epidermal stem cell clusters by Notch-mediated lateral induction. *Dev. Biol.* **258**, 141–153. (doi:10.1016/S0012-1606(03)00107-6)

23 Altand, A. & Simons, B. D. 2010 *Condensed matter field theory*, 2nd edn. Cambridge, UK: Cambridge University Press. (doi:10.1017/CBO9780511789984)

24 Cross, M. C. & Hohenberg, P. C. 1993 Pattern formation outside equilibrium. *Rev. Mod. Phys.* **65**, 851–1112. (doi:10.1103/RevModPhys.65.851)

25 Lara-Ochoa, F. 1984 A generalized reaction diffusion model for spatial structure formed by motile cells. *Biosystems* **17**, 35–50. (doi:10.1016/0303-2647(84)90014-5)
26 Glotzer, S. C., Di Marzio, E. A. & Muthukumar, M. 1995 Reaction-controlled morphology of phase-separating mixtures. *Phys. Rev. Lett.* **74**, 2034–2037. (doi:10.1103/PhysRevLett.74.2034)
27 Cahn, J. W. & Hilliard, J. E. 1958 Free energy of a nonuniform system. I. Interfacial free energy. *J. Chem. Phys.* **28**, 258–267. (doi:10.1063/1.1744102)
28 Elliott, C. M. & Garcke, H. 1997 Diffusional phase transitions in multicomponent systems with a concentration dependent mobility matrix. *Physica D* **109**, 242–256. (doi:10.1016/S0167-2789(97)00066-3)
29 Klein, A. M., Doupé, D. P., Jones, P. H. & Simons, B. D. 2007 Kinetics of cell division in epidermal maintenance. *Phys. Rev. E* **76**, 021 910. (doi:10.1103/PhysRevE.76.021910)
30 Bray, A. J. 1994 Theory of phase-ordering kinetics. *Adv. Phys.* **43**, 357–459. (doi:10.1080/00018739400101505)
31 Murray, J. D. 2003 *Mathematical biology*, vol. 2, 3rd edn. Berlin, Germany: Springer.
32 Klein, A. M., Doupé, D. P., Jones, P. H. & Simons, B. D. 2008 Mechanism of murine epidermal maintenance: cell division and the Voter model. *Phys. Rev. E* **77**, 031 907. (doi:10.1103/PhysRevE.77.031907)
33 Giacomin, G. & Lebowitz, J. L. 1996 Exact macroscopic description of phase segregation in model alloys with long range interactions. *Phys. Rev. Lett.* **76**, 1094–1097. (doi:10.1103/PhysRevLett.76.1094)
34 Domany, E. & Kinzel, W. 1984 Equivalence of cellular automata to Ising models and directed percolation. *Phys. Rev. Lett.* **53**, 311. (doi:10.1103/PhysRevLett.53.311)
35 Gillespie, D. 1976 General method for numerically simulating stochastic time evolution of coupled chemical-reactions. *J. Comp. Phys.* **22**, 403. (doi:10.1016/0021-9991(76)90041-3)